Euroasia Journal of Mathematics, Engineering, Natural & Medical Sciences
International Indexed and Refereed
ISSN 2667-6702

A Computational Study on 1, 4-Benzodioxane-Substituted Chalcone Derivative

Sümeyya Serin*

Dr., Inonu University, Scientific and Technological Research Center, 44280, Malatya, Türkiye

** Corresponding author: sumeyya.alatas@inonu.edu.tr*

Geliş Tarihi / Received: 13.09.2023
Kabul Tarihi / Accepted: 30.09.2023

Araştırma Makalesi/ Research Article
DOI: 10.5281/zenodo.10373784

ABSTRACT

In this present study, a benzodioxane substituted chalcone derivative was investigated in aqueous solution and gas phase using calculations based on density functional theory (DFT). After optimizing the geometry of the molecule by using the B3LYP functional and 6-311++G(d,p) split-valence triple zeta basis set, experimental and theoretical structural parameters were compared and found to be compatible. The FT-IR analysis revealed that the experimental and theoretical results of C-H, C=O, and C=C stretching vibrations overlapped. Several quantum chemical reactivity descriptors were calculated and interpreted for both vacuum and water phases by means of HOMO and LUMO energies determined as a result of frontier molecular orbital (FMO) theory analysis. In order to characterize various intramolecular interactions and to estimate the corresponding stabilization energies, analysis of natural bond orbitals (NBO) was performed. As a result of the in-silico lipophilicity evaluation of the aforementioned chalcone derivative, the n-octanol/water partition coefficient ($logP_{ow}$) was calculated as 3.57. Therefore, it can be concluded that the molecule has lipophilic character. This finding is also supported by the molecular lipophilicity potential (MLP) map.

Keywords: Chalcone, lipophilicity, DFT, NBO

1. INTRODUCTION

Chalcones have gained a popular place in organic synthesis due to their tremendous pharmacological activities and photo-physical properties (Nayak et al., 2023; Katariya, et al., 2023). Due to their wide range of pharmacological activities, which are schematized in Figure 1, studies on the synthesis of new chalcone derivatives and the examination of their activities have been emphasized in recent years (Kınalı et al., 2023; Lakhia et al., 2023; Thapa et al., 2021). In addition, it is noteworthy that related studies are supported by quantum chemical methods. This study deals with a benzodiaoxane substituted chalcone derivative whose synthesis and crystal structure were described by Vinaya et al. Further, Vinaya et al. elucidated the chemical structure of the mentioned derivative using various spectroscopic techniques such as ^{1}H-NMR, ^{13}C-NMR and FT-IR (Vinaya et al., 2023). In addition to these studies, herein, the relevant compound was examined from a theoretical perspective. In this context, quantum chemical-based calculations were performed on the chalcone derivative and its molecular structure was optimized. Experimental FT-IR data were compared with data obtained from DFT calculations. NBO analysis was completed by examining intramolecular donor-acceptor orbital interactions and estimating the stabilization energy values corresponding to these interactions. Considering the pharmacological activities of chalcone derivatives (Figure 1), the reactivity indices of the molecule and lipophilicity evaluation, which is an important factor in terms of bioavailability, were also included in the scope of the study.

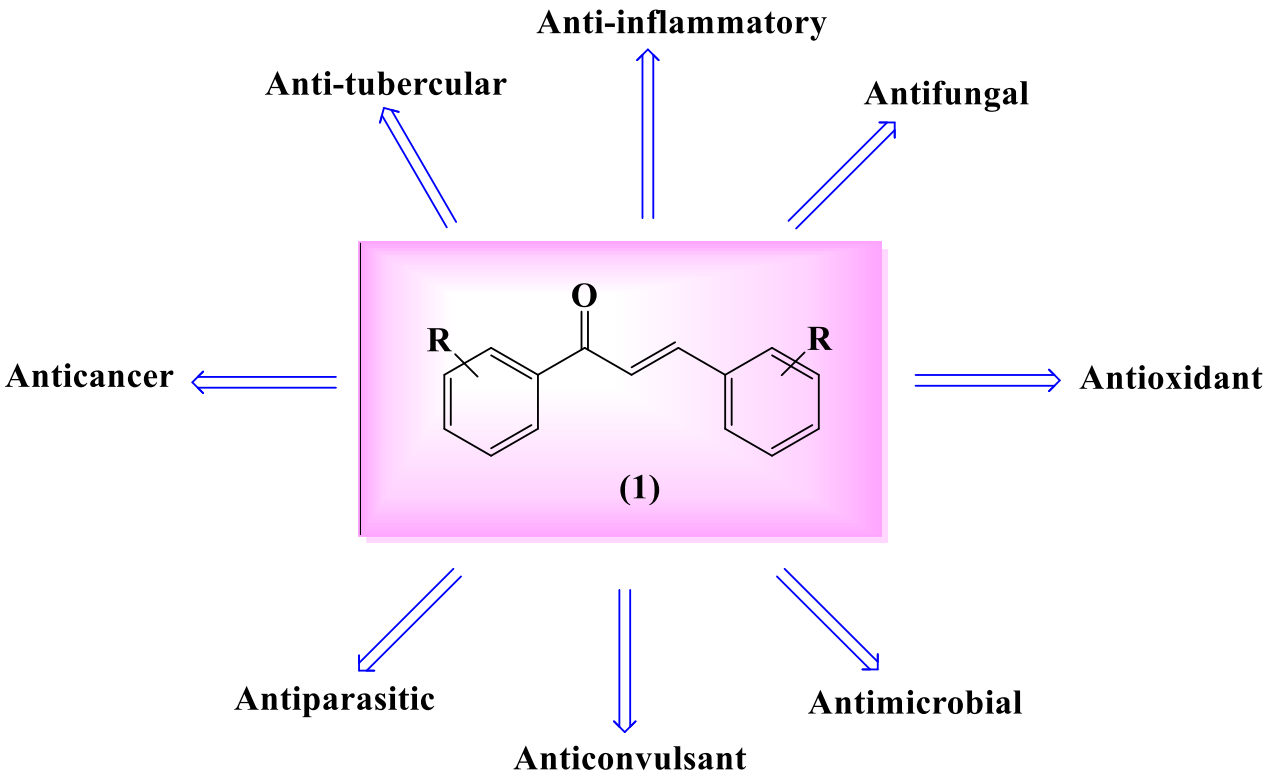

Figure 1. Various pharmacological activities of chalcones

2. COMPUTATIONAL THEORY

The geometry of studied chalcone derivative was completely optimized using GAUSSIAN 16 software package (Frisch et al., 2016) on applying the B3LYP functional and the 6-311++G (d, p) basis set (Becke, 1993; Becke, 1993, Lee et al., 1988). Gauss View 6 software (Dennington et al., 2016) was utilized for illustrations of the optimized structure, FMO, and MEP diagrams. The density of states (DOS) plot was visualized by Gauss-Sum 3.0 program (O'Boyle et al., 2008). The water phase (ε=78.4) calculations were carried out by using the universal implicit SMD (**S**olvent **M**odel based on **D**ensity) model in order to examine the impact of bulk solvent (Marenich et al., 2009). For all computations, optimized structures were verified by the absence of imaginary frequency. In order to evaluate basic physicochemical and lipophilicity characteristics, SwissADME software (Daina et al., 2017) was utilized. The n-octanol/water partition coefficient ($logP_{ow}$) was determined utilizing five different methodologies, which were ILOGP, XLOGP3, WLOGP, MLOGP, and SILICOS-IT. Additionally, molecular lipophilicity potential (MLP) maps of studied compound were visualized in Molinspiration Galaxy 3D Structure Generator v2018.01 beta (https://www.molinspiration.com; Gaillard et al., 1994).

In accordance with Koopmans theorem (Koopmans, 1934), ionization energy (I) ($I= - E_{HOMO}$) and electron affinity (A) ($A= -E_{LUMO}$) values can be specified by HOMO and LUMO energies. In addition, some DFT-based reactivity parameters of the related compound were calculated within the scope of the study. The definitions and formulas of the mentioned parameters are presented below (equations (1)-(4)) (Parr and Pearson, 1983; Pearson, 1986; Parr, 1999; Perdew and Levy, 1983; Perdew et al., 1982).

Chemical Potential	$\mu = -\frac{I + A}{2}$	(1)
Chemical Hardness	$\eta = \frac{I - A}{2}$	(2)
Electronegativity	$\chi = \frac{I + A}{2}$	(3)
Electrophilicity index	$\omega = \frac{\mu^2}{2\eta}$	(4)

NBO analysis of the studied compound was carried out by using the second-order Fock matrix (Weinhold et al., 2016; Reed et al., 1988) at DFT/B3LYP/6–311++G (d, p) methodology. In this way, donor-acceptor orbital interactions and stabilization energy predictions were examined. Stabilization energies were computed according to the formula designated in equation (5). The formula components can be explained as follows: $E^{(2)}$: Stabilization energy, qi: Donor orbital occupancy, Fij: Off diagonal Fock matrix, εi and εj: diagonal element, donor and acceptor orbital energies.

$$E^{(2)} = \Delta E_{ij} = qi\left[\frac{(Fij)^2}{(\varepsilon j - \varepsilon i)}\right] \quad (5)$$

3. RESULTS and DISCUSSION

Molecular Geometry

The optimized structure of studied chalcone derivative was obtained by using DFT/B3LYP/6-311++G (d, p) methodology. The numbered and labeled structure of the respective compound is visualized and presented in Figure 2. The overlapped version of the experimental structure with the calculated structure is also shown in Figure 2. Selected optimized geometrical parameters are compiled in Table 1. Computed parameters were compared with experimental values given in the literature (Vinaya et al., 2023).

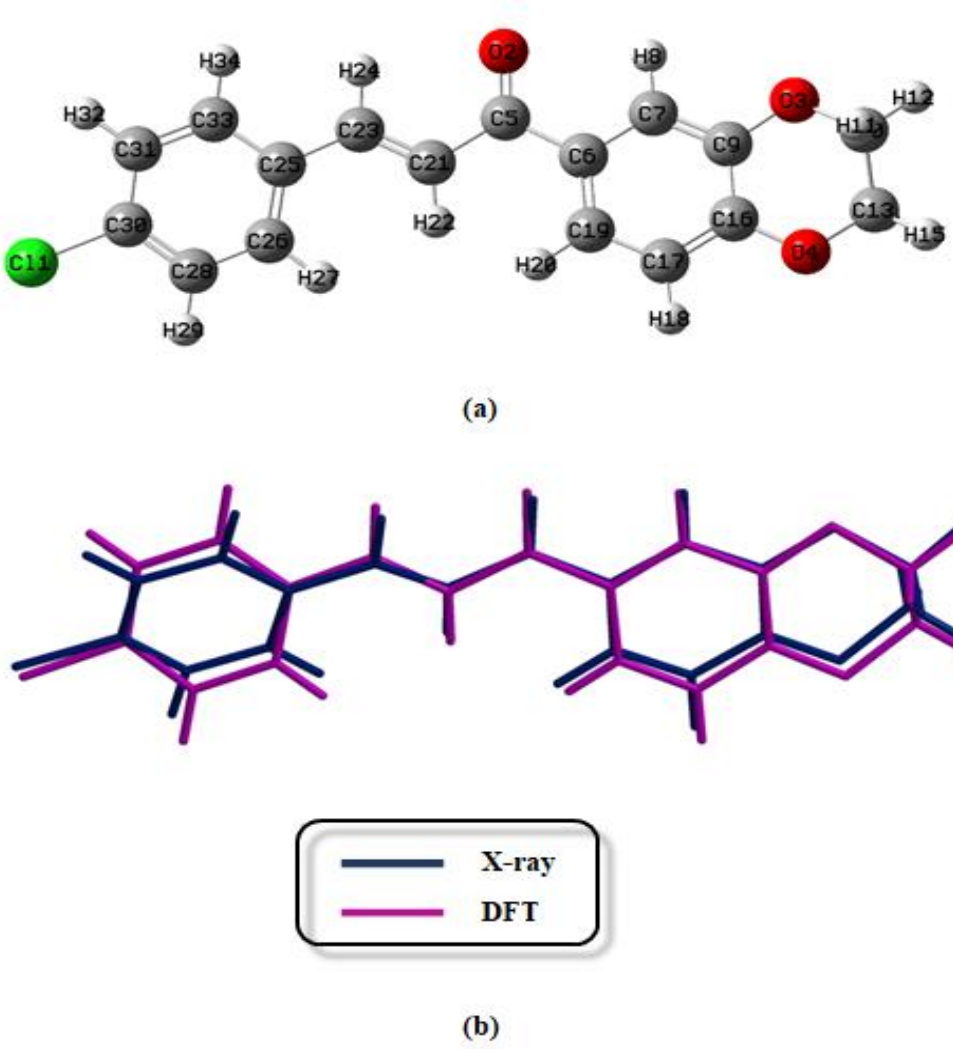

Figure 2. Optimized molecular structure of the studied compound calculated at ground state (a); superimposition of DFT and X-ray structure (b)

Table 1. Selected optimized structural parameters

Bond Length (Å)	**Exp.**	**DFT**	**Bond Length (Å)**	**Exp.**	**DFT**
O2-C5	1.229	1.225	C6-C7	1.396	1.400
O3-C9	1.372	1.372	C23-C25	1.465	1.461
O3-C10	1.433	1.429	C25-C26	1.397	1.406
O4-C16	1.366	1.366	C25-C33	1.399	1.404
C5-C21	1.480	1.486	C17-C19	1.388	1.384
Bond Angle (°)	**Exp.**	**DFT**	**Bond Angle (°)**	**Exp.**	**DFT**
C16-O4-C13	114.7	114.6	C5-C6-C7	117.9	117.3
O2-C5-C21	121.2	120.8	C5-C6-C19	123.7	123.9
O2-C5-C6	120.0	120.1	C7-C9-C16	119.9	119.7
C21-C5-C6	118.8	118.9	O3-C10-C13	110.0	110.1
C7-C6-C19	118.4	118.6	Cl1-C30-C31	119.3	119.6
Dihedral Angle (°)	**Exp.**	**DFT**	**Dihedral Angle (°)**	**Exp.**	**DFT**
C26-C28-C30-C31	0.9	0.1	C16-C17-C19-C6	-0.8	-0.9
C26-C28-C30-Cl1	-179.0	-179.9	C7-C5-C19-C17	-0.2	-0.2
C5-C6-C7-C9	179.1	179.6	C5-C6-C19-C17	-178.6	-179.6
O4-C16-C17-C19	-179.9	-179.2	O3-C10-C13-O4	-60.1	-60.7
C9-C16-C17-C19	1.3	1.4	O3-C9-C16-C17	179.0	179.1

As indicated in Table 1, the calculated bond lengths, bond angles, and dihedral angles are in agreement with the literature. Four different O-C bond lengths were calculated in the range of 1.225-1.429 Å. While O2-C5, O3-C9, O3-C10, and O4-C16 bond lengths were calculated as 1.225, 1.372, 1.429, and 1.366 Å respectively, these distances were reported as 1.229, 1.372, 1.433, and 1.366 Å experimentally. Also, selected C-C bond lengths were calculated in the range of 1.384-1.486 Å. On the other hand, considering the bond angles, it was observed that the C-C-C angles varied between 117.3-123.9 ̊. The dihedral angles C26-C28-C30-C31 and C26-C28-C30-Cl1 were predicted as 0.1˚and -179.9˚ respectively. Experimental values of related angles were reported as 0.9˚ and -179.9˚. Also, O3-C10-C13-O4 and O3-C9-C16-C17 angles were computed as -60.7˚ and 179.1̊, while they were recorded as -60.1˚and 179.0˚experimentally.

FT-IR Characterization

FT-IR spectroscopy takes part among the widely used methods to identify the functional groups and bond structures of a given molecule. The vibrational analysis of the studied chalcone derivative was carried out in the gas phase at B3LYP/6-311++G (d,p) theory level. However, a scaling factor is used to balance for the difference between experimental and theoretical vibrational frequencies. Herein, the computed frequencies were scaled with a factor of 0.983 for the 4000-1700 cm^{-1} region and 0.958 for the 1700-0 cm^{-1} region (Sundaraganesan et al., 2005). The FT-IR spectrum of the respective compound obtained by DFT calculations is presented in Figure 3. Additionally, some selected computed approximate frequencies (unscaled and scaled) along with their IR intensities and probable assignments were exhibited in Table 2.

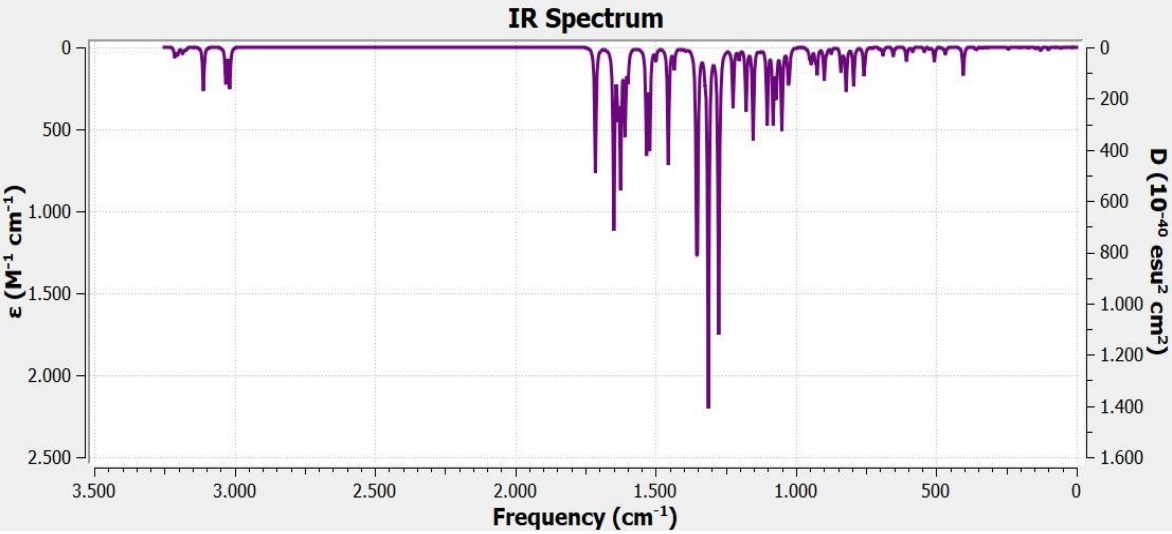

Figure 3. Computed IR spectrum of studied chalcone derivative

As indicated in Table 2, Ar-CH stretching vibration modes were computed as 3158, 3150, 3148, 3131, and 3119 cm^{-1}. These vibrations were experimentally recorded in the region of 3156-2934 cm^{-1} (Vinaya et al., 2023). The symmetric and asymmetric vibrations of the dioxane ring were estimated in the 3059-2966 cm^{-1} range. C=O vibrations, which were determined experimentally in the region of 1655 cm^{-1}, were calculated in the range of 1685-1556 cm^{-1} theoretically. On the other hand, while C=C vibrations were calculated in the range of 1685-1468 cm^{-1}, the experimental data

point to 1575 cm^{-1}. Scissoring, wagging, rocking, and twisting vibrations of the CH_2 groups of the dioxane ring were also clearly indicated in the table.

Table 2. Computed approximate vibrational frequencies (in cm^{-1}) of studied chalcone derivative

Assignment	Exp.	I_{IR}	Unscaled	Scaled
νCH (Ar-CH)		13	3213	3158
νCH (Ar-CH)	3156	7	3204	3150
νCH (Ar-CH)		2	3202	3148
νCH (Ar-CH)		8	3185	3131
νCH (Ar-CH)		4	3173	3119
$\nu_{as}CH_2$ (dioxane ring)		16	3112	3059
$\nu_{as}CH_2$ (dioxane ring)		42	3110	3057
$\nu_{as}CH_2$ (dioxane ring)		47	3031	2979
νCH_2 (dioxane ring)	2934	53	3017	2966
νCO + νCC		165	1714	1685
νCO + νCC	1655	236	1648	1579
νCO + νCC		72	1634	1565
νCO + νCC		175	1624	1556
νCC + ipb HCC	1575	107	1608	1540
νCC + ipb HCC		37	1598	1531
νCC + ipb HCC		134	1532	1468
νCC + ipb HCC		127	1521	1457
δ CH_2		12	1499	1436
δ CH_2		4	1497	1434
δ CH_2 + νCC + ipb HCC		154	1454	1393
ω CH_2		1	1408	1349
ω CH_2		3	1393	1334
ω CH_2 + νCC + ipb HCC		183	1354	1297
νCC + ipb HCC		182	1350	1293
τ CH_2 + νCC+ ring breathing		471	1312	1257
τ CH_2 + νCC+ ring breathing		374	1275	1221
ρ CH_2		3	1122	1075
νC-Cl + ipb HCC		100	1102	1056
νC-O + ipb HCC		96	1081	1036
νC-O + ipb HCC		58	1070	1025
opb HCC		28	1023	980
opb HCC + ρ CH_2		19	945	905
opb HCC		32	839	804

Abbreviations; I_{IR}: IR intensity, Ar: Aromatic; ν: symmetric stretching, ν_{as}: asymmetric stretching, ω: wagging, δ: scissoring, τ: twisting, ρ: rocking ipb: in plane bending, opb: out of plane bending

FMO Theory and MEP Analysis

Molecular orbital theory, which has an important role in understanding electronic properties and chemical reactions, is a frequently studied subject especially in the field of computational chemistry. The frontier molecular orbitals are generally utilized in order to describe the location of electron transfer from HOMO to LUMO of the molecule. The energy gap value ($\Delta E = E_{LUMO}$-E_{HOMO}) of a particular molecule is a substantial parameter in the chemical stability and reactivity evaluations of that molecule. For the studied chalcone derivative, HOMO & LUMO energies, energy gaps, and some DFT-based reactivity parameters computed according to equations (1)-(4) and their variations according to water environment are listed in Table 3. As observed in Table 3, the energy gap values (ΔE) for the vacuum and water phases were calculated as 3.82 eV and 3.65 eV, respectively. It was observed that the chemical hardness value (η) decreased when passing from the vacuum to the water phase. Vacuum and water phase values were estimated as 1.91 eV and 1.83 eV. Moreover, the electrophilicity index value of the water phase (5.44 eV) of the studied compound was calculated slightly higher than that of the gas phase (5.14 eV). This indicates the better electrophilic nature of the derivative in the aqueous environment.

Table 3. The computed DFT-based reactivity parameters (in eV)

	E_{HOMO}	E_{LUMO}	ΔE	η	μ	χ	ω
Vacuum	-6.34	-2.52	3.82	1.91	-4.43	4.43	5.14
Water	-6.28	-2.63	3.65	1.83	-4.46	4.46	5.44

Figure 4 exhibits three-dimensional HOMO-LUMO diagrams of the respective compound along with the DOS graph. In respect of Figure 4, it is evident that HOMO densities are spread over the entire molecule. Similarly, LUMO densities (antibonding character) are spread throughout the molecule except for the O3 atom and CH_2 groups of the dioxane ring.

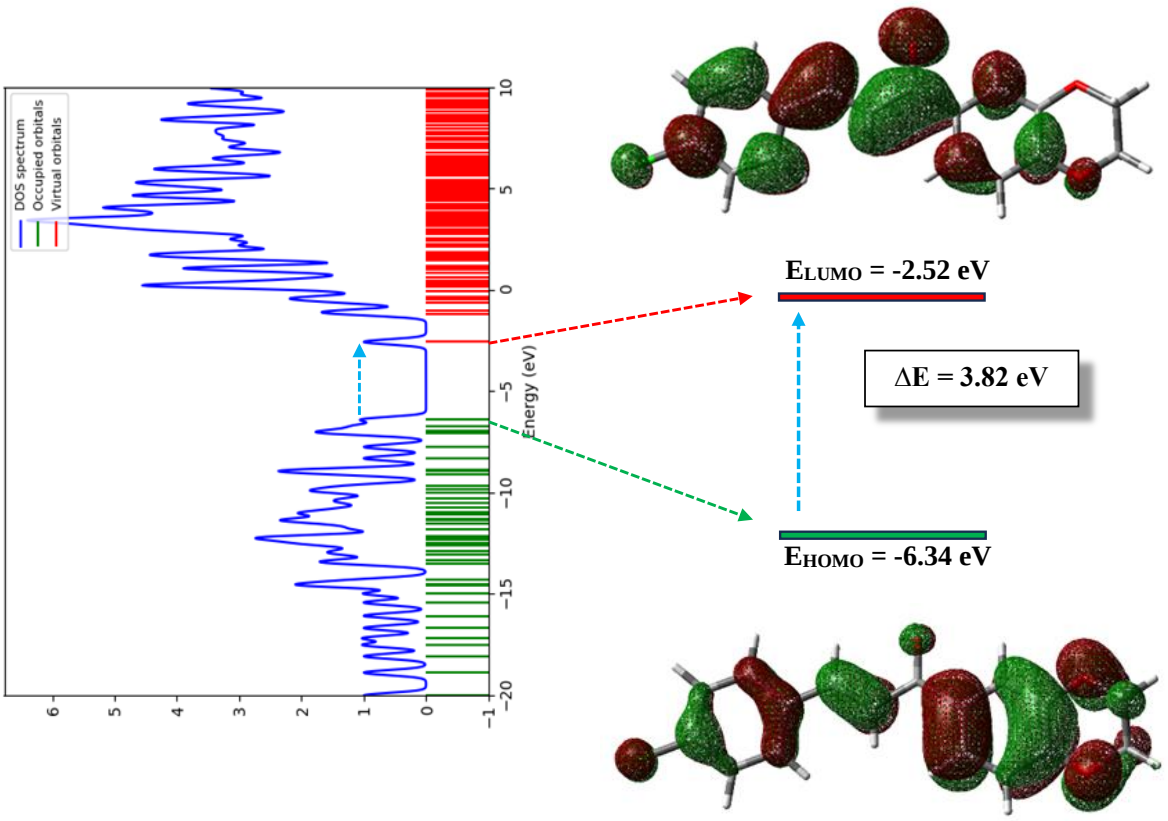

Figure 4. HOMO-LUMO (isoval: 0.02) and DOS diagrams of studied compound

Molecular electrostatic potential (MEP) mapping is an effective technique that shows the electrostatic potential regions of a given molecule and the regions vulnerable to nucleophilic or electrophilic attack by color grading. Figure 5 shows the MEP surface maps of the related compound. Different values of electrostatic potential are indicated by different colors. Generally, on the color scale of MEP maps, red designates high electron density, blue designates low electron density, and yellow and green designate intermediate levels. The molecular electrostatic potentials of studied chalcone are in the range of -0.005492 a.u (deepest red) - +0.005492 a.u. (deepest blue) in gas phase. It was observed that the positive potentials were mostly concentrated around the hydrogen atoms, while the negative potentials were mainly concentrated on the O2 atom.

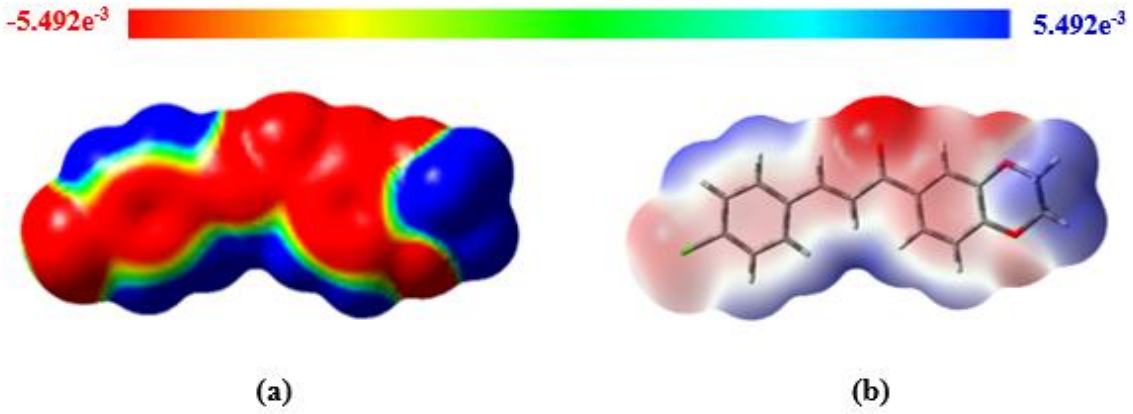

Figure 5. MEP (isoval: 0.0004) diagrams of examined chalcone derivative; solid form (a), transparent form (b)

NBO Analysis

In this part of the study, NBO analysis of the investigated chalcone derivative was carried out using the DFT/B3LYP/6-311++G (d,p) methodology. Interactions between the bonding and antibonding orbitals of the molecule were evaluated. Table 4, which is prepared by considering the stabilization energies of the molecule greater than 10 kcal/mol, includes the occupancy rates of the bonding/antibonding orbitals along with the significant interactions. LP represents lone pairs. When Table 4 is examined, σ→σ*, π→π*, and LP→π* interactions stand out. It is obvious that σ→σ* interactions with stabilization energies varying between 10.76-32.34 kcal/mol are more predominant. Considering C-C (π→π*) resonance energies, the stabilization energies of π (C25-C33) (ED_i = 1.61460e) → π* (C26-C28) (ED_j = 0.29199e), π (C26-C28) (ED_i = 1.68273e) → π* (C25-C33) (ED_j = 0.37282e), π (C30-C31) (ED_i = 1.67105e) → π* (C25-C33) (ED_j = 0.37282e), and π (C30-C31) (ED_i = 1.67105e) → π* (C26-C28) (ED_j = 0.29199e) interactions were determined as 15.01, 18.41, 19.25, and 17.10 kcal/mol respectively. In addition, the interactions between a lone-pair orbital on C6 atom, LP (1) C6, and antibonding acceptors π* O2-C5 (52.06 kcal/mol), π* C7-C9 (73.96 kcal/mol), and π* C17-C19 (80.85 kcal/mol) orbitals exhibited high stabilization energies.

Table 4. Principal findings of the NBO study

Donor(i)	ED_i/e	Acceptor(j)	ED_j/e	$E^{(2)}$ kcal/mol	E(j)-E(i)/a.u	F(i.j)/a.u
σ Cl1-C30	1.98875	σ* C23-C25	0.02393	12.44	0.34	0.058
σ C6-C7	1.96770	σ* C10-H12	0.01417	22.64	0.37	0.082
		σ* C17-H18	0.01307	11.60	0.56	0.072
		σ* C23-C25	0.02393	27.97	0.31	0.084
σ C6-C19	1.97472	π* C26-C28	0.29199	14.94	0.96	0.115
σ C7-H8	1.97329	σ* C10-H12	0.01417	14.51	0.18	0.046
		σ* C19-H20	0.01388	13.42	0.23	0.049
		σ* C23-C25	0.02393	21.40	0.13	0.047
σ C10-H11	1.98432	σ* C23-C25	0.02393	13.57	0.16	0.041
σ C10-H12	1.97924	σ* C6-C7	0.01986	21.18	0.82	0.117
σ C10-C13	1.99108	σ* C10-H12	0.01417	14.41	0.33	0.062
σ C21-H22	1.97785	σ* C10-H12	0.01417	12.13	0.20	0.044
		σ* C23-C25	0.02393	26.44	0.15	0.056
σ C21-C23	1.97928	σ* C6-C7	0.01986	12.25	0.98	0.098
		σ* C23-C25	0.02393	32.34	0.36	0.096
π C21-C23	1.84237	π* O2-C5	0.21639	18.83	0.31	0.070

Donor(i)	ED_i/e	Acceptor(j)	ED_i/e	$E^{(2)}$ kcal/mol	E(j)-E(i)/a.u	F(i.j)/a.u
		π* C25-C33	0.37282	12.09	0.29	0.056
σ C23-H24	1.97262	σ* Cl1-C30	0.03279	10.76	0.55	0.069
σ C23-C25	1.97550	σ* Cl1-C30	0.03279	16.06	0.71	0.095
π C25-C33	1.61460	π* C21-C23	0.10475	16.52	0.30	0.068
		π* C26-C28	0.29199	15.01	0.32	0.063
σ C26-H27	1.97878	σ* C10-H12	0.01417	16.20	0.20	0.051
		σ* C19-H20	0.01388	13.19	0.25	0.051
		σ* C23-C25	0.02393	16.82	0.15	0.045
σ C26-C28	1.97113	σ* C17-H18	0.01307	19.70	0.58	0.096
π C26-C28	1.68273	π* C25-C33	0.37282	18.41	0.29	0.066
σ C28-H29	1.97856	σ* Cl1-C30	0.03279	11.16	0.62	0.075
σ C30-C31	1.97971	σ* Cl1-C30	0.03279	11.19	0.79	0.084
π C30-C31	1.67105	π* C25-C33	0.37282	19.25	0.30	0.069
		π* C26-C28	0.29199	17.70	0.34	0.070
σ C31-H32	1.97830	σ* Cl1-C30	0.03279	17.10	0.58	0.089
σ C31-C33	1.97081	σ* Cl1-C30	0.03279	17.80	0.80	0.107
LP (2) O2	1.88784	σ* C5-C6	0.06395	18.79	0.68	0.102
LP (2) O3	1.86244	π* C7-C9	0.34890	22.30	0.35	0.084
LP (1) C6	1.05272	π* O2-C5	0.21639	52.06	0.15	0.098
		π* C7-C9	0.34890	73.96	0.14	0.107
		π* C17-C19	0.33619	80.85	0.12	0.107

Lipophilicity Analysis

Lipophilic nature of the mentioned chalcone derivative was evaluated by utilizing SwissADME and Molinspiration software. Both web tools are freely accessible and easy to use. Table 5 was created with the data obtained as a result of in silico analysis. Numerical predictions of the physicochemical and lipophilic characteristics of the relevant compound are included in the table. Accordingly, the polar surface area of the molecule was calculated as 35.53 Å², while the molar refractivity value was predicted as 82.13. The water solubility properties were calculated according to three different approaches. According to ESOL (Delaney, 2004) and Ali (Ali et al., 2012), the molecule is in the soluble class, on the other hand, according to the SILICOS-IT (https://www.silicos-it.be) approach, it is considered moderately soluble. The partition coefficient of a particular molecule in the n-octanol/water solvent system is the conventional model used to determine the lipophilic nature of that molecule. The $logP_{ow}$ value was determined utilizing five different methodologies, which were ILOGP, XLOGP3, WLOGP, MLOGP, and SILICOS-IT. The values were estimated as 3.23, 3.25, 3.90, 2.77, and 4.72 respectively. The consensus logP (average of five predictive models) was determined as 3.57, which indicates the lipophilic behavior of the chalcone derivative. On the other hand, Figure 6 provides a visual of the lipophilic potential of the molecule. Lipophilicity results can be highlighted with molecular lipophilicity potential (MLP) maps. As indicated in the Figure 6, the blue and purple regions represent lipophilic interactions. The green regions concentrated on the dioxane ring indicate intermediate lipophilic interactions. In support of the SwissADME results, the MLP map also confirms the lipophilic character.

Table 5. Estimation of physicochemical properties, water solubility, and $logP_{ow}$ values

Physicochemical properties		Water Solubility		Lipophilicity	
Molecular weight (g/mol)	300.74	Log S (ESOL)	-3.98	Log $P_{o/w}$ (iLOGP)	3.23
Num. heavy atoms	21	Solubility (mg/mL)x10^{-2}	3.17	Log $P_{o/w}$ (XLOGP3)	3.25
Num. arom. heavy atoms	12	Class	Soluble	Log $P_{o/w}$ (WLOGP)	3.90
Fraction Csp3	0.12	Log S (Ali)	-3.67	Log $P_{o/w}$ (MLOGP)	2.77
Num. rotatable bonds	3	Solubility (mg/mL)x10^{-2}	6.43	Log $P_{o/w}$ (SILICOS-IT)	4.72
Num. H-bond acceptors	3	Class	Soluble	Consensus Log $P_{o/w}$	3.57
Num. H-bond donors	0	Log S (SILICOS-IT)	-5.59		
Molar Refractivity	82.13	Solubility (mg/mL)x10^{-4}	7.73		
TPSA (Å²)	35.53	Class	Moderately soluble		

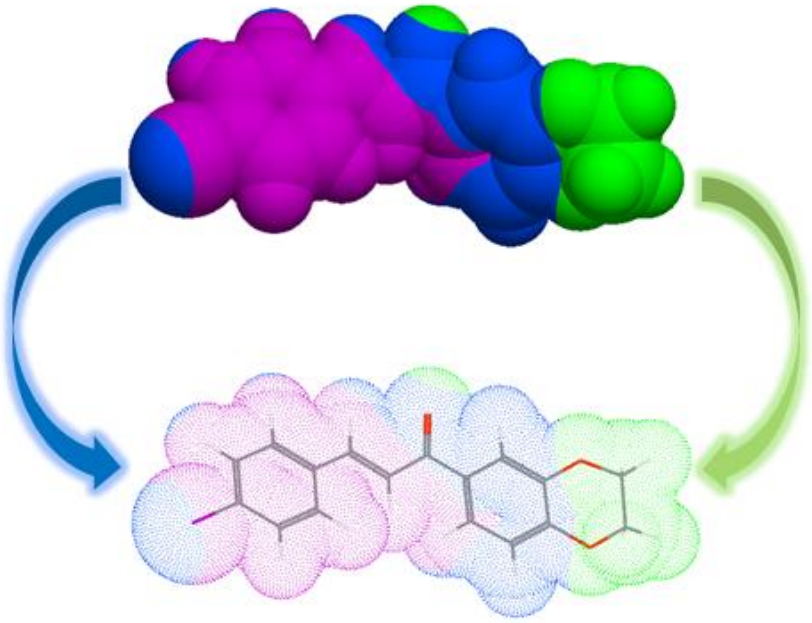

Figure 6. MLP maps of studied compound

4. CONCLUSION

This study includes the theoretical research results of the spectroscopic, electronic and lipophilic properties of the synthesized benzodioxane substituted chalcone derivative. For theoretical research, SwissADME and Molinspiraton software as well as DFT-based calculations performed via Gaussian software were utilized. The optimized molecular structure was superimposed with the molecular structure obtained from X-ray analysis. Besides, the geometrical parameters were compared and they were determined to be compatible. FT-IR spectrum, DOS diagram, and HOMO-LUMO plots were visualized and the data obtained from the calculations were interpreted. Quantum chemical reactivity descriptors were calculated for both vacuum and water phases and the reactivity behavior was examined. Electrostatic surface properties and molecular lipophilicity potential were examined by mapping technique using color codes. From here, nucleophilic and electrophilic attack sites and lipophilic interaction sites were determined. $LogP_{ow}$ value was estimated at 3.57. Therefore, it is evident that numerical and visual predictions of lipophilic character confirm each other.

ACKNOWLEDGEMENT

The numerical calculations reported in this paper were partially performed at TUBITAK ULAKBIM, High Performance and Grid Computing Center (TRUBA resources).

REFERENCES

Ali, J., Camilleri, P., Brown, M. B., Hutt, A. J., & Kirton, S. B. (2012). In Silico Prediction of Aqueous Solubility Using Simple QSPR Models: The Importance of Phenol and Phenol-like Moieties. Journal of Chemical Information and Modeling, 52, 2950−2957.

Becke A.D. (1993). A new mixing of Hartree–Fock and Local Density-Functional Theories, Journal of Chemical Physics, 98, 1372–1377.

Becke A.D. (1993). Density-Functional Thermochemistry. III. The Role of Exact Exchange, Journal of Chemical Physics, 98, 5648–5652.

Daina, A.; Michielin, O.; Zoete, V. (2017). SwissADME: A Free Web Tool to Evaluate Pharmacokinetics, Drug-likeness and Medicinal Chemistry Friendliness of Small Molecules, Scientific Reports, 7(1), 1.

Delaney, J. S. (2004). ESOL: Estimating Aqueous Solubility Directly from Molecular Structure. Journal of Chemical Information and Computer Sciences, 44, 1000-1005.

Dennington, R.; Keith, T. A.; Millam, J. M. GaussView, Version 6 Semichem Inc., Shawnee Mission, KS. 2016.

Frisch, M. J.; Trucks, G. W.; Schlegel, H. B.; Scuseria, G. E. et.al. Gaussian 16 Rev. B.01, Wallingford, CT, 2016.

Gaillard P., Carrupt P.A., Testa B., Boudon A. (1994). Molecular Lipophilicity Potential, a tool in 3D QSAR: Method and applications, Journal of Computer-Aided Molecular Design, 8, 83.

Katariya, K.D., Soni, R., Nakum, K.J., Patel, D., Nada, S., Hagar, M. (2023). New Symmetric/Unsymmetrical Self-assembling Salicylaldimine-Chalcones: Synthesis, Photophysical Study and DFT Approach, Journal of Molecular Structure, 136610.

Kınalı, M., Çol, S., Çakır Çoban, C., Türk, M., Aydın, G., Emirik, M., Baran, A. (2023). Chalcone-Based Dipolar Cycloaddition of Novel Heteroaromatic Compounds: Their Anticancer Examination, Journal of Molecular Structure 1293, 136244.

Koopmans, T. (1934). Über die zuordnung von wellenfunktionen und eigenwerten zu den einzelnen elektronen eines atoms, Physica, 1–6, 104–113

Lakhia, R., Verma, N.K., Raghav, N., Pundeer, R. (2023). Chalcone and Pyrazoline Derivatives of Dehydroacetic Acid as Digestive Enzyme Effectors and In Silico Studies, Journal of Molecular Structure 1291, 135884.

Lee C., Yang W., Parr R.G. (1988). Development of the Colle-Salvetti Correlation-Energy Formula into a Functional of the Electron Density, Physical Review B 37, 785–789.

Marenich A.V., Cramer C.J., Truhlar D.G. (2009). Universal Solvation Model Based on Solute Electron Density and on a Continuum Model of the Solvent Defined by the Bulk Dielectric Constant and Atomic Surface Tensions, Journal of Physical Chemistry B, 113 (18), 6378-6396.

Molinspiration Cheminformatics free web services, https://www.molinspiration.com, Slovensky Grob, Slovakia.

Nayak, Y.N., Gaonkar, S.L., Sabu, M. (2023). Chalcones: Versatile Intermediates in Heterocyclic Synthesis, Journal of Heterocyclic Chemistry, 60:1301–1325.

O'Boyle N. M., Tenderholt A. L. Langer K. M. (2008). Cclib: A Library for Package-Independent Computational Chemistry Algorithms, Journal of computational chemistry, 29 (5), 839-45.

Parr, R.G. (1999). Electrophilicity index, Journal of American Chemical Society, 121,1922-1924.

Parr, R.G., Pearson, R.G. (1983). Absolute hardness: companion parameter to absolute electronegativity, Journal of American Chemical Society, 105, 7512-7516.

Pearson, R.G. (1986). Absolute electronegativity and hardness correlated with molecular orbital theory, Proceedings of the National Academy of Sciences USA, 83, 8440-8441.

Perdew J.P., Levy M. (1983). Physical content of the exact kohn-sham orbital energies: band gaps and derivative discontinuities, Physical Review Letters, 51, 1884-1887.

Perdew J.P., Parr R.G., Levy M., Balduz J.L. (1982). Density-functional theory for fractional particle number: derivative discontinuities of the energy, Physical Review Letters, 49, 1691.

Reed A.E., Curtiss L.A., Weinhold F. (1988). Intermolecular interactions from a natural bond orbital, donor-acceptor viewpoint, Chemical. Reviews. 88(6), 899-926

Silicos-it. (n.d.). Retrieved from https://www.silicos-it.be

Sundaraganesan N., Ilakiamani S., Salem H., Wojciechowski P.M., Michalska D. (2005). FT-Raman and FT-IR spectra, vibrational assignments and density functional studies of 5-bromo-2-nitropyridine, Spectrochimica Acta, Part A: Molecular and Biomolecular Spectroscopy, 61, 2995–3001.

Thapa, P., Upadhyay, S.P., Suo, W.Z., Singh, V., Gurung, P., Lee, E.S., Sharma, R., Sharma, M. (2021). Chalcone and Its Analogs: Therapeutic and Diagnostic Applications in Alzheimer's Disease, Bioorganic Chemistry 108, 104681.

Vinaya, Richard, A.S., Murthy, S.M., Basavaraju, Y.B., Yathirajana H.S., Parkin, S. (2023). The Synthesis, Crystal Structure and Spectroscopic Analysis of (E)-3-(4-chlorophenyl)-1-(2,3-dihydrobenzo[b][1,4]dioxin-6-yl)prop-2-en-1-one, Acta Crystallographica Section E: Crystallographic Communications, E79, 674–677.

Weinhold F., Landis C.R., Glendening E.D. (2016). What is NBO analysis and how is it useful, International Reviews in Physical Chemistry, 35, 399-440.